Structural Engineering and Mechanics, Vol. 43, No. 4 (2012) 459-473
DOI: http://dx.doi.org/10.12989/sem.2012.43.4.459

Longitudinal anti-cracking analysis for post-tensioned voided slab bridges

Zhen Zhou*, Shao-ping Meng[a] and Zhao Liu[b]

Key Laboratory of RC&PC of Ministry of Education, Southeast University, Nanjing, 210096, China

(Received October 31, 2010, Revised May 16, 2012, Accepted August 7, 2012)

Abstract. Post-tensioned concrete voided slab girders are widely used in highway bridge constructions. To obtain greater section hollow rate and reduce the self-weight, the plate thickness of slab girders are designed to be small with the adoption of flat anchorage system. Since large prestress is applied to the anchor end section, it was found that longitudinal shear cracks are easy to occur along the voided slab girder. The reason is the existence of great shearing effect at the junction area between web and bottom (top) plate in the anchor end section. This paper focuses on the longitudinal anti-cracking problem at the anchor end of post-tensioned concrete voided slab girders. Two possible models for longitudinal anti-cracking analysis are proposed. Differential element analysis method is adopted to derive the solving formula of the critical cracking state, and then the practical analysis method for longitudinal anti-cracking is established. The influence of some factors on the longitudinal anti-cracking ability is studied. Results show that the section dimensions (thickness of bottom, web and top plate) and prestress eccentricity on web plate are the main factors that influence the anti-cracking ability. Moreover, the proposed method is applied into three engineering examples to make longitudinal anti-cracking verification for the girders. According to the verification results, the design improvements for these girders are determined.

Keywords: voided slab girder bridge; post-tensioned concrete; anchor end; longitudinal anti-cracking; critical cracking state

1. Introduction

Voided slab girders have advantages such as low girder height, light self-weight, convenient fabrication and erection, and great mechanical performance. Because of that, they are commonly used in construction of interstate bridges with medium and small spans (Jáuregui *et al.* 2010). Moreover, when prestress is applied, the height of voided slab girders can be further reduced, the under-bridge space increased, and the mechanical performance improved. Therefore, prestressed voided slab girders are widely used in highway bridges (Zhao *et al.* 2007).

Since voided slab girders are widely used in practical bridge construction, many scholars and engineers have made a lot of research on their analysis method, mechanical performance and

*Corresponding author, Associate Professor, E-mail: seuhj@163.com
[a]Professor, E-mail: Cardoso_meng@sina.com
[b]Professor, E-mail: mr.liuzhao@seu.edu.cn

optimal design. In particular, Sen *et al.* (1993) gtested to failure two voided slab bridge models, one straight and the other one curved in plan, under simulated AASHTO truck loading. Lounis *et al.* (1995) illustrated the application of an effective optimization procedure for the design of prestressed concrete cellular bridge decks consisting of single and two-cell voided slab systems. Optimization results showed that voided slab decks are more economical than box girder decks for short span ranges and wide bridge decks. O'Brien *et al.* (1998) used upstanding finite element method to analyze voided slab bridge decks with wide transverse edge cantilevers. This method is sufficiently simple to be used on an everyday basis in the design office. In order to calculate prestress losses in the transverse prestressing of voided concrete slabs, Jaeger *et al.* (1998) reviewed a simple expression for calculating the equivalent thickness specified by Canadian Highway Bridge Design Code, and a simple alternative expression, believed to be more accurate, is proposed, along with its derivation. Mari *et al.* (2000) described the geometric characteristics, conceptual design, analysis and construction of a new type of continuous precast concrete girder and voided slab bridge deck, and discussed particular aspects related to the influence of the segmental construction on the structural behavior at service of this type of voided slab bridge. Scollard *et al.* (2004) illustrated rehabilitation criteria and the application of checking procedures for post-tensioned voided-slab bridges through example calculations for a typical continuous bridge. Connor *et al.* (2008) present the application of probabilistic techniques to the load capacity assessment of an existing post-tensioned concrete slab bridge. Qaqish *et al.* (2009) made comparison between computed shearing forces by AASHTO specifications and the finite element method of two continuous spans of a voided slab bridge. Results show that the maximum shear obtained by both methods are found to be in good agreement, with negligible differences. Díaz *et al.* (2010) presented a computer software which allows the generation of a complete structural model of a concrete bridge with a voided slab deck, a common design for medium span bridges.

In recent years, to obtain greater section hollow rate and reduce the self-weight, a new type of flat anchorage system is introduced into post-tensioned voided slab girders. Fig. 1~Fig. 3 show an application example of the girder anchor section with this system in Suqian-Huaian Expressway design of Jiangsu Province, China. As shown in Fig. 3, the flat anchorage system is adopted in both web and bottom plate. Since the flat anchorage is much thinner than regular ring anchorage, the thickness of the web and bottom plate could be reduced greatly. However, when the large prestress is applied through flat anchorage, the longitudinal deformation of the web, bottom and top plate could be different, for their different geometry and prestress value. As a result, great shearing effect

Fig. 1 Suqian-Huaian Expressway

Fig. 2 Post-tensioned voided slab girders with flat anchorage

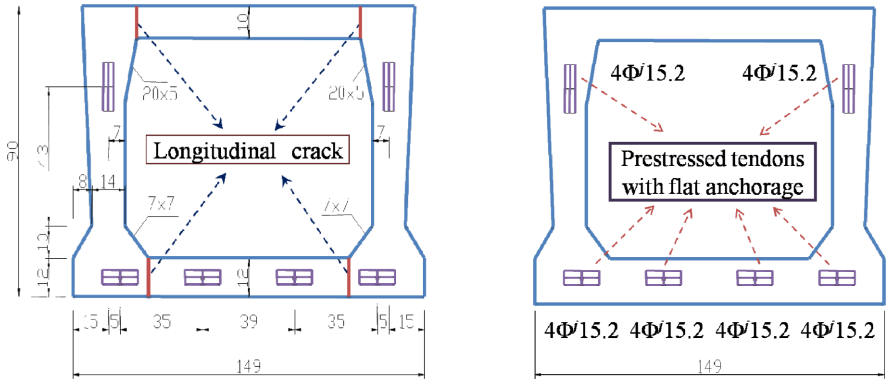

Fig. 3 Anchor end section and longitudinal crack of slab girders with flat anchorage system (unit: cm)

may occur at the junction area between the web plate and bottom (top) plate. Great principal tensile stress is then easily generated at these locations. If the principal tensile stress exceeds the limit value, the longitudinal shear crack along the girder will occur. Not only can the service performance of the bridge structure be influenced, but also the structural damage may occur finally. Therefore, an appropriate method should be developed to evaluate the longitudinal anti-cracking ability at the anchorage end of the voided slab girder.

In this paper, pointing to the character of section geometry and prestress at the anchor end, two possible models of longitudinal anti-cracking analysis are proposed for post-tensioned concrete voided slab girders with flat anchorage system. The differential element analysis method is adopted to derive the solving formula of the critical cracking state, and then the practical analysis method for longitudinal anti-cracking is established to provide theoretical basis and a practical method for the design of this type of prestressed voided slab girders.

2. Theoretical analysis of the longitudinal anti-cracking

2.1 Fundamental assumption

When making the theoretical analysis of longitudinal anti-cracking for post-tensioned concrete voided slab girder with flat anchorage system, the following assumptions are adopted:

(1) Concrete is homogeneous, linear elastic, and of the same nature throughout the bridge.
(2) Shear strain between the web, top and bottom plates change linearly along the girder.
(3) Friction between the girder and the support is not considered.
(4) Section geometry and prestress at the anchor end are bilaterally symmetrical.

2.2 Analytical model

Fig. 3 shows the section of a prestressed voided slab girder with 20 m span which is used in the Suqian-Huaian express highway. The top of web plate on either side of the girder is equipped with a bunch of four 1860 MPa-grade prestressed steel strands with a bending angle of 7.5°, while the bottom of web plate is equipped with a bunch of four straight strands. The total prestress for the

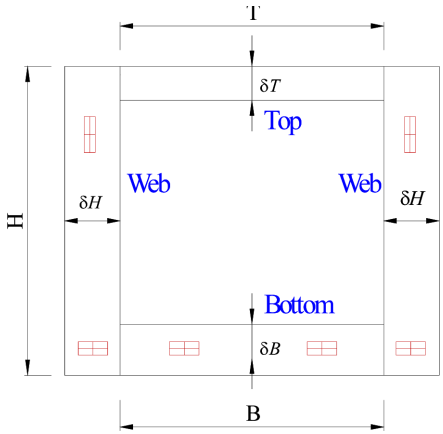

Fig. 4 Equivalent section of the prestressed voided slab girder

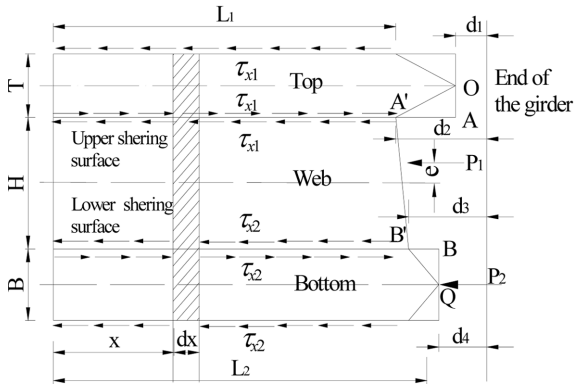

Fig. 5 Analytical model A

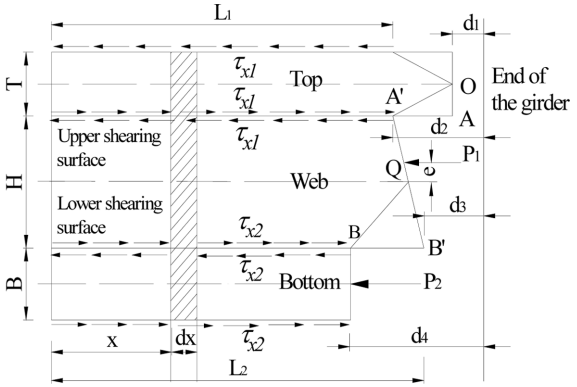

Fig. 6 Analytical model B

tendons on the web plate is 1562.4 kN. The bottom plate is equipped with 2 bunches of 4 straight linear prestressed steel strands, and the total prestress for tendons on the bottom plate is also 1562.4 kN. For the convenience of making longitudinal analysis, the girder section in Fig. 3 is transformed into the equivalent section shown in Fig. 4 according to the area equivalent principle. Besides, based on the section form and the prestress distribution, two possible longitudinal anti-cracking analysis models are proposed, which are shown in Fig. 5 and Fig. 6.

According to Saint-Venant principle, the prestress applied on the anchor end has a non-uniform influence only in a relatively small range. Therefore, the mutual shearing effect length between the web and top plate (upper shearing face) is supposed to be L_1, and the one between the web and bottom plate (lower shearing face) is L_2. Since the section geometry and prestress at the anchor end are bilaterally symmetrical (assumption (4) in part 2.1), the shearing stress along longitudinal crack should be bilaterally symmetrical. Therefore, only one side web plate and its neighboring top, bottom plates are intercepted within the shearing effecting length for analysis. Fig. 5 and Fig. 6 show two possible analytical models. The left side of two models is considered as fixed end. The total prestress force imposed on the one-side web plate is P_1, and its eccentricity to the centroid of the web plate is e. The prestress on the bottom plate is P_2, located at the centroid of the bottom plate.

2.3 Differential element analysis

In the analytical model, a differential segment at a distance of x from the left end is analyzed. Considering the effect of reinforcement on the shearing face, the compressed deformation under the effect of shearing stress on both sides of top plate is

$$d_1 = \int_0^{L_1} \frac{N_x}{ET\delta_T} dx = \int_0^{L_1} \frac{2\int_x^{L_1} \tau_{x1}\delta_B dx + \sum_{i=1}^{n_{x1}} \tau_{i1}A_{gi1}}{ET\delta_T} dx = \frac{2}{ET}\int_0^{L_1}\int_x^{L_1} \tau_{x1} dx + \frac{L_1}{ET\delta_T}\sum_{i=1}^{n_1} \tau_{i1}A_{gi1} \tag{1}$$

Under the effect of prestress and shearing stress on both sides, the compressed deformation at the top of the web plate is:

For analytical model A

$$\begin{aligned} d_2^{(A)} &= \int_0^{L_1}\left(\frac{P_1}{EH\delta_H} + \frac{P_1 eH}{2EI_H}\right)dx - \frac{1}{EH\delta_H}\left(\int_0^{L_1} N_{x1}dx - \int_0^{L_2} N_{x2}dx\right) - \left(\int_0^{L_1} N_{x1}dx + \int_0^{L_2} N_{x2}dx\right)\frac{H^2}{4EI_H} \\ &= \int_0^{L_1}\left(\frac{P_1}{EH\delta_H} + \frac{6P_1 e}{EH^2\delta_H}\right)dx - \frac{4\delta_T}{EH\delta_H}\int_0^{L_1}\left(\int_x^{L_1}\tau_{x1}dx\right)dx - \frac{2\delta_B}{EH\delta_H}\int_0^{L_2}\left(\int_x^{L_2}\tau_{x2}dx\right)dx \\ &\quad - \frac{4L_1}{EH\delta_H}\sum_{i=1}^{n_1}\tau_{i1}A_{gi1} - \frac{2L_2}{EH\delta_H}\sum_{i=1}^{n_2}\tau_{i2}A_{gi2} \end{aligned} \tag{2-a}$$

For analytical model B

$$\begin{aligned} d_2^{(B)} &= \int_0^{L_1}\left(\frac{P_1}{EH\delta_H} + \frac{P_1 eH}{2EI_H}\right)dx - \frac{1}{EH\delta_H}\left(\int_0^{L_1} N_{x1}dx + \int_0^{L_2} N_{x2}dx\right) - \left(\int_0^{L_1} N_{x1}dx - \int_0^{L_2} N_{x2}dx\right)\frac{H^2}{4EI_H} \\ &= \int_0^{L_1}\left(\frac{P_1}{EH\delta_H} + \frac{6P_1 e}{EH^2\delta_H}\right)dx - \frac{4\delta_T}{EH\delta_H}\int_0^{L_1}\left(\int_x^{L_1}\tau_{x1}dx\right)dx + \frac{2\delta_B}{EH\delta_H}\int_0^{L_2}\left(\int_x^{L_2}\tau_{x2}dx\right)dx \\ &\quad - \frac{4L_1}{EH\delta_H}\sum_{i=1}^{n_1}\tau_{i1}A_{gi1} + \frac{2L_2}{EH\delta_H}\sum_{i=1}^{n_2}\tau_{i2}A_{gi2} \end{aligned} \tag{2-b}$$

where E is the elastic modulus of concrete; τ_{i1} and τ_{i2} are the shearing stresses of reinforcement; A_{gi1} and A_{gi2} are the transformed section area of the reinforcement (the original section area of the reinforcement multiply the elastic modulus ratio of steel to concrete); $\delta_T, T, \delta_B, B, \delta_H, H$ are the thickness of the top plate, width of the top plate, thickness of the bottom plate, width of the bottom plate, thickness of the web plate, and width of the web plate, respectively; $I_H = \delta_H H^3/12$ is the sectional inertia moment of the web plate; n_{x1} and n_{x2} are the number of reinforcements on the two shearing faces in the range from x-section to girder end, and n_1 and n_2 are the ones in the range of L_1 and L_2.

The compressed deformation at the bottom of web plate due to the prestress and the shearing stress on both sides is:

For analytical model A

$$d_3^{(A)} = \int_0^{L_1}\left(\frac{P_1}{EH\delta_H}-\frac{P_1eH}{2EI_H}\right)dx-\frac{1}{EH\delta_H}\left(\int_0^{L_1}N_{x1}dx-\int_0^{L_2}N_{x2}dx\right)+\left(\int_0^{L_1}N_{x1}dx+\int_0^{L_2}N_{x2}dx\right)\frac{H^2}{4EI_H}$$

$$= \int_0^{L_1}\left(\frac{P_1}{EH\delta_H}-\frac{6P_1e}{EH^2\delta_H}\right)dx+\frac{2\delta_T}{EH\delta_H}\int_0^{L_1}\left(\int_x^{L_1}\tau_{x1}dx\right)dx+\frac{4\delta_B}{EH\delta_H}\int_0^{L_2}\left(\int_x^{L_2}\tau_{x2}dx\right)dx$$

$$+\frac{2L_1}{EH\delta_H}\sum_{i=1}^{n_1}\tau_{i1}A_{gi1}+\frac{4L_2}{EH\delta_H}\sum_{i=1}^{n_2}\tau_{i2}A_{gi2} \tag{3-a}$$

For analytical model B

$$d_3^{(B)} = \int_0^{L_1}\left(\frac{P_1}{EH\delta_H}-\frac{P_1eH}{2EI_H}\right)dx-\frac{1}{EH\delta_H}\left(\int_0^{L_1}N_{x1}dx+\int_0^{L_2}N_{x2}dx\right)+\left(\int_0^{L_1}N_{x1}dx-\int_0^{L_2}N_{x2}dx\right)\frac{H^2}{4EI_H}$$

$$= \int_0^{L_1}\left(\frac{P_1}{EH\delta_H}-\frac{6P_1e}{EH^2\delta_H}\right)dx+\frac{2\delta_T}{EH\delta_H}\int_0^{L_1}\left(\int_x^{L_1}\tau_{x1}dx\right)dx-\frac{4\delta_B}{EH\delta_H}\int_0^{L_2}\left(\int_x^{L_2}\tau_{x2}dx\right)dx$$

$$+\frac{2L_1}{EH\delta_H}\sum_{i=1}^{n_1}\tau_{i1}A_{gi1}-\frac{4L_2}{EH\delta_H}\sum_{i=1}^{n_2}\tau_{i2}A_{gi2} \tag{3-b}$$

It can be seen from the expressions of d_2 and d_3 that the influence of the bending moment caused by prestress eccentricity and shearing force eccentricity are both considered.

The compressed deformation of bottom plate caused by prestress and the shearing stress on both sides is:

For analytical model A

$$d_4^{(A)} = \int_0^{L_2}\frac{P_2-N_x}{EB\delta_B}dx = \int_0^{L_2}\frac{P_2}{EB\delta_B}dx-\frac{2}{EB}\int_0^{L_2}\left(\int_x^{L_2}\tau_{x2}dx\right)dx-\frac{L_2}{EB\delta_B}\sum_{i=1}^{n_2}\tau_{i2}A_{gi2} \tag{4-a}$$

For analytical model B

$$d_4^{(B)} = \int_0^{L_2}\frac{P_2+N_x}{EB\delta_B}dx = \int_0^{L_2}\frac{P_2}{EB\delta_B}dx+\frac{2}{EB}\int_0^{L_2}\left(\int_x^{L_2}\tau_{x2}dx\right)dx+\frac{L_2}{EB\delta_B}\sum_{i=1}^{n_2}\tau_{i2}A_{gi2} \tag{4-b}$$

2.4 Relation between prestress P and shearing length L

In Fig. 5 and Fig. 6, it is supposed that the straight line OA and QB remains straight after the deformation of top and bottom plates. Then, the stress-strain relation before the cracking at point A(A') and B(B') is

$$\tau_A = G\gamma_A, \quad \tau_B = G\gamma_B \tag{5}$$

where, G is the shearing elastic modulus of concrete; τ_A and τ_B are the shear stresses at point A and B; γ_A and γ_B are the shear strains at point A and B. Based on the geometric deformation relationship, it can be obtained that:

For analytical model A

$$\gamma_A^{(A)} = 2(d_2^{(A)} - d_1)/T, \quad \gamma_B^{(A)} = 2(d_4^{(A)} - d_3^{(A)})/H \tag{6-a}$$

For analytical model B

$$\gamma_A^{(B)} = 2(d_2^{(B)} - d_1)/T, \quad \gamma_B^{(B)} = 2(d_3^{(B)} - d_4^{(B)})/B \tag{6-b}$$

Substitute Eq. (6) into Eq. (5), it can be concluded that:

For analytical model A

$$d_2^{(A)} - d_1 = \frac{T\tau_A}{2G}, \quad d_4^{(A)} - d_3^{(A)} = \frac{H\tau_A}{2G} \tag{7-a}$$

For analytical model B

$$d_2^{(B)} - d_1 = \frac{T\tau_A}{2G}, \quad d_3^{(B)} - d_4^{(B)} = \frac{B\tau_A}{2G} \tag{7-b}$$

According to the fundamental assumption (3), $\gamma_{x1} = \frac{x}{L_1}\gamma_A$, $\gamma_{x2} = \frac{x}{L_2}\gamma_B$, then

$$\tau_{x1} = G\gamma_{x1} = \frac{x}{L_1}G\gamma_A = \frac{x}{L_1}\tau_A \tag{8-a}$$

$$\tau_{x2} = G\gamma_{x2} = \frac{x}{L_2}G\gamma_B = \frac{x}{L_2}\tau_B \tag{8-b}$$

Therefore

$$\int_0^{L_1}\int_x^{L_1}\tau_{x1}dx = \int_0^{L_1}\int_x^{L_1}\frac{x}{L_1}\tau_{A1}dx = \frac{\tau_A L_1^2}{3} \tag{9-a}$$

$$\int_0^{L_2}\int_x^{L_2}\tau_{x2}dx = \int_0^{L_1}\int_x^{L_1}\frac{x}{L_2}\tau_{A2}dx = \frac{\tau_B L_2^2}{3} \tag{9-b}$$

$$\sum_{i=1}^{n_1}\tau_{i1}A_{gi1} = \sum_{i=1}^{n_1}\frac{x_{i1}}{L_1}\tau_{A1}A_{gi1} = \frac{\tau_A}{L_1}\sum_{i=1}^{n_1}x_{i1}A_{gi1} \tag{10-a}$$

$$\sum_{i=1}^{n_1}\tau_{i2}A_{gi2} = \sum_{i=1}^{n_1}\frac{x_{i1}}{L_1}\tau_{A2}A_{gi2} = \frac{\tau_B}{L_1}\sum_{i=1}^{n_1}x_{i2}A_{gi2} \tag{10-b}$$

Substitute Eq. (1)~Eq. (4) and Eq. (9)~Eq. (10) into Eq. (7), it can be obtained as following

$$P_1 = abL_1 + acL_2^2L_1^{-1} + adL_1^{-1} \tag{11}$$

$$P_2 = a'fP_{1a} + a'b'L_2 + a'c'L_1^2L_2^{-1} + a'd'L_2^{-1} \tag{12}$$

where the coefficients of Eq. (11) and Eq. (12) can be expressed as following

$$a=\frac{EH^2\delta_H}{H+6e};\quad b=\frac{2H\delta_H+4T\delta_T}{3ETH\delta_H}\tau_A;\quad a'=EB\delta_B;\quad c'=\frac{2\delta_T}{3EH\delta_H}\tau_A;\quad f=\frac{H-6e}{EH^2\delta_H} \tag{13-a}$$

For analytical model A

$$c^{(A)}=\frac{2\delta_B}{3EH\delta_H}\tau_B;\quad d^{(A)}=\frac{T}{2G}\tau_A+\frac{2\sum_{i=1}^{n_2}x_{i2}A_{gi2}}{EH\delta_H}\tau_B+\frac{H\delta_H+4T\delta_T}{EHT\delta_H\delta_T}\tau_A\sum_{i=1}^{n_1}x_{i1}A_{gi1}$$

$$b'^{(A)}=\frac{2H\delta_H+4B\delta_B}{3EBH\delta_H}\tau_B;\quad d'^{(A)}=\frac{H}{2G}\tau_A+\frac{2\sum_{i=1}^{n_2}x_{i1}A_{gi1}}{EH\delta_H}\tau_A+\frac{H\delta_H+4B\delta_B}{EHB\delta_H\delta_B}\tau_B\sum_{i=1}^{n_1}x_{i2}A_{gi2} \tag{13-b}$$

For analytical model B

$$c^{(B)}=-\frac{2\delta_B}{3EH\delta_H}\tau_B;\quad d^{(B)}=\frac{T}{2G}\tau_A-\frac{2\sum_{i=1}^{n_2}x_{i2}A_{gi2}}{EH\delta_H}\tau_B+\frac{H\delta_H+4T\delta_T}{EHT\delta_H\delta_T}\tau_A\sum_{i=1}^{n_1}x_{i1}A_{gi1}$$

$$b'^{(B)}=-\frac{4B\delta_B+2H\delta_H}{3EBH\delta_H}\tau_B;\quad d'^{(B)}=-\frac{B}{2G}\tau_A+\frac{2\sum_{i=1}^{n_2}x_{i1}A_{gi1}}{EH\delta_H}\tau_A-\frac{H\delta_H+4B\delta_B}{EHB\delta_H\delta_B}\tau_B\sum_{i=1}^{n_1}x_{i2}A_{gi2} \tag{13-c}$$

2.5 Solution to critical cracking state

The objective is to solve the critical cracking prestress P_{1cr} and P_{2cr}. When the section is in the critical longitudinal cracking state, major tensile stress σ_{ZL} at point A(A') and B(B') should reach the limit value. At this moment, there is only shearing stress on the discussed shearing face. Therefore, at point A (A') and (B'), $\tau_A=\sigma_{ZLA}$ or $\tau_B=\sigma_{ZLB}$. Then, from Eq. (11) and Eq. (12), it can be concluded that P_1 and P_2 are only functions of L_1 and L_2 in the critical longitudinal cracking state. P_{1cr} and P_{2cr} should be the smallest solution to make the stress in shearing face reach the limit value.

According to the Chinese Bridge Standard, the major tensile stress should meet the requirement $\sigma_{ZL}\le 1.3f_t$ (f_t is the tensile strength of concrete), that is $\tau_A=1.3f_t$ or $\tau_B=1.3f_t$ before the section cracking. But the relation between τ_A and τ_B can not be determined. Therefore, a correlation coefficient ρ is introduced to describe the mutual relation between the shearing state of upper shearing face and bottom shearing face when the section is in the critical cracking state. If $\rho=0$, the upper and lower shearing faces are completely unrelated. In other words, when the upper (lower) shearing face is in the critical cracking state, the shearing stress and the shearing effect length on the lower (upper) shearing face are both 0. If $\rho=1$, the upper and lower shearing faces are completely related, and reach the critical cracking state at the same time. At this time, $\tau_A=\tau_B=1.3f_t$, L_1 and L_2 both reach the critical shearing effect length. Therefore, P_{1cr} and P_{2cr} can be obtained respectively when $\rho=0$ and $\rho=1$.

Actually, the real value of ρ should be between 0 and 1. Therefore, the real value for P_{1cr} and P_{2cr} should be between the solutions of $\rho=0$ and $\rho=1$. Therefore, a solution interval for P_{1cr} and P_{2cr}

can be obtained. Although in this way, the exact value of P_{1cr} and P_{2cr} can not be calculated, it is still rather important to evaluate the longitudinal anti-cracking capability of the girder section and also provide important guide for the anchor end design.

(i) Case 1: $\rho = 1$, at this time,

Based on $\frac{dP_{2cr}}{dL_2} = a'b' - a'(c'L_1^2 + d')/L_2^2 = 0$, it can be concluded as following

$$L_2 = \sqrt{(c'L_1^2 + d')/b'} \tag{14}$$

Substitute Eq. (14) into Eq. (11)

$$P_1 = a(b + cc'/b')L_1 + a(d + cd'/b')L_1^{-1} \tag{15}$$

Based on $\frac{dP_1}{dL_1} = 0$, it can be calculated that

$$L_1 = \sqrt{\frac{db' + cd'}{bb' + cc'}} \tag{16}$$

According to Eq. (16), L_1 can be obtained. Substitute the solution of L_1 into Eq. (14) and Eq. (15), L_2 and P_{1cr} can be worked out. Then, according to Eq. (12), P_{2cr} can be obtained.

(ii) Case 2: $\rho = 0$, at this time:

For P_{1cr}, $\tau_B = 0, L_2 = 0$. Based on $\frac{dP_1}{dL_1} = 0$, it can be concluded that

$$L_1 = \sqrt{\frac{d}{b}} \quad P_{1cr} = 2a\sqrt{bd} \tag{17}$$

For P_{2cr}, $\tau_A = 0, L_1 = 0$, based on $\frac{dP_2}{dL_1} = 0$, it can be obtained as following

$$L_2 = \sqrt{\frac{d'}{b'}}, \quad P_{2cr} = a'fP_{1cr} + 2a'\sqrt{b'd'} \tag{18}$$

According to Eq. (17) and Eq. (18), P_{1cr} and P_{2cr} can be obtained.

It should be noted that only the shear reinforcements within the range of shearing effect length L_1 and L_2 can take the shear-resistant effect. That means that the number of reinforcement taking real shear-resistant effect can not be known in advance. However, this should be known for solving L_1 and L_2. Therefore, in the calculating process, the value of L_1 and L_2 obtained without considering shear reinforcement effect is used as initial value. Then through iterative calculation, the exact value of L_1, L_2 and P_{1cr}, P_{2cr} can be obtained.

3. Influence of various factors on the cracking critical prestress

As shown in the various coefficient expressions of Eq. (11) and Eq. (12), the factors that have

influence on critical cracking prestress include: prestress eccentricity on the web plate, section dimension at the anchor end of the voided slab girder and the shear reinforcement settled on shearing faces. Moreover, when designing the section dimensions of the girder anchor end, the thickness of bottom, web and top plates are usually the most important parameters.

According to the analysis method proposed in this paper, the MATLAB numerical analysis software is adopted to compile the longitudinal anti-cracking analysis program (John *et al.* 2005). Then, the relation between $\overline{P}_{cr}$ (middle value of the critical cracking prestress solution interval) and various influencing factors is obtained, which is shown in Fig. 7~Fig. 11 (the direction of eccentricity e is assumed to be positive in Fig. 5 and Fig. 6). In the program, the central parameters are $E = 3.45 \times 10^4$ MPa, $G = 1.41 \times 10^4$ MPa, $B = 0.91$ m, $\delta_B = 0.12$ m, $T = 0.95$, $\delta_T = 0.1$ m, $H = 0.9$ m, $\delta_H = 0.2$ m, $e = -0.04$, and $A_{s1} = 0$ (supposing that on the up and bottom shearing faces, the line spacing of shear reinforcements is 10 cm, and the section area of each-line shear reinforcement

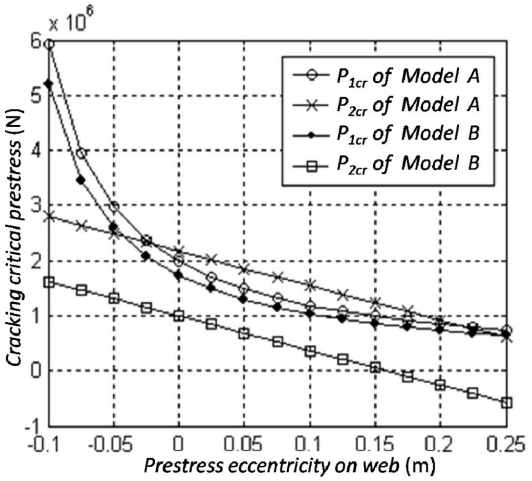

Fig. 7 $\overline{P}_{cr} - e$ curve

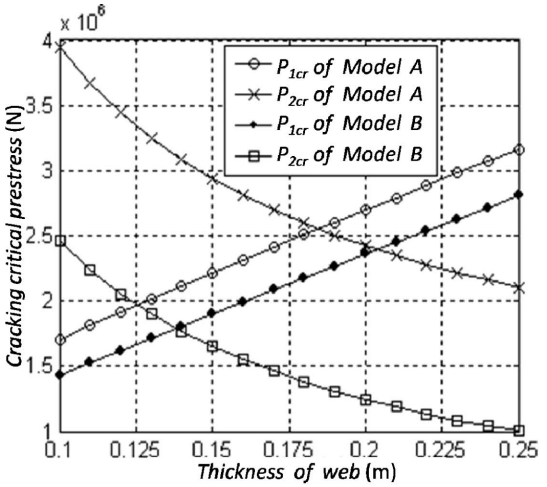

Fig. 8 $\overline{P}_{cr} - \delta_H$ curve

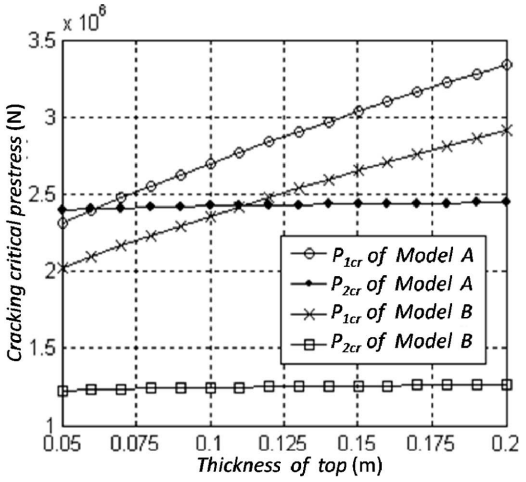

Fig. 9 $\overline{P}_{cr} - \delta_T$ curve

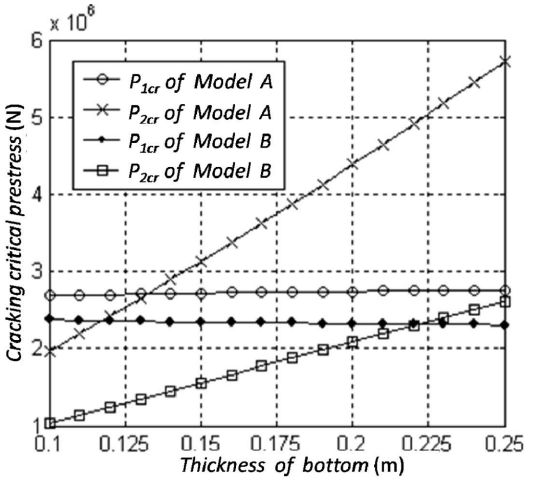

Fig. 10 $\overline{P}_{cr} - \delta_B$ curve

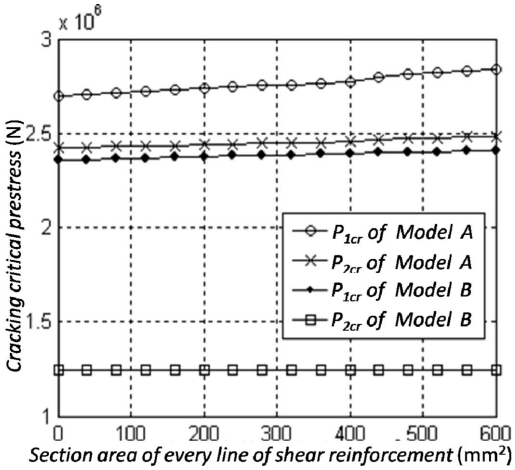

Fig. 11 $\overline{P}_{cr} - A_{s1}$ curve

is A_{s1}). Every single influential factor is made to change each time, and the changing tendency of $\overline{P}_{cr}$ with that influential factor is obtained.

It can be seen from Fig. 7~ Fig. 11:

(1) The analytical results of Model A and Model B are different. The final critical cracking prestress should be the minimum value between the solutions of the two models. Moreover, from Fig. 9, it should be noticed that the solved value of critical cracking prestress could be negative, which is not real in actual engineering. When making the longitudinal anti-cracking analysis, it is recommended that full analysis is made to both Model A and Model B, if the analytical model can not be surely determined (in very special cases can be determined before analysis, shown in part 4.2 and 4.3). Then the final critical cracking prestress is the minimum positive value of the solutions.

(2) In both Model A and Model B, the increase of positive eccentricity has negative effects on the longitudinal anti-cracking capability, while the increase of negative eccentricity improves the longitudinal anti-cracking capability greatly. The increase of bottom plate thickness has great positive influence on P_{2cr}, while has little influence on P_{1cr}. The increase of top plate thickness has great positive influence on P_{1cr}, while has little influence on P_{2cr}. Moreover, the increase of web plate thickness makes P_{1cr} increase, but makes P_{2cr} decrease.

(3) In both analytical models, with the increase of shearing reinforcement section area, P_{1cr} and P_{2cr} both increase, but with a little amplitude. The reason is that when shearing face comes to critical state, the limited value of shearing stress is relatively small. As a result, the tensile stress that shear reinforcement bears is small. Moreover, the area of shear reinforcement equivalent into concrete is not large. Therefore, the influence and effect of shearing reinforcement is limited.

4. Longitudinal anti-cracking verification for engineering examples

4.1 The girder of Suqian-Huaian Expressway

As shown in Fig. 1, for the section of prestress voided slab girder in Suqian-Huaian Expressway, $E = 3.45 \times 10^4$ MPa, $G = 1.41 \times 10^4$ MPa, $f_t = 1.71$ MPa, $B = 0.91$ m, $\delta B = 0.12$ m, $T = 0.95$, $\delta T =$

0.1 m, H = 0.9 m, δH = 0.2 m, and e = –0.04 m. There is not shear reinforcement settled on the shearing face, that is A_{s1} = 0. Since the prestress is applied on both the web and bottom plate, the cracking model can not be determined in advance. Therefore, full analysis should be made to Model A and Model B. According to the compiled longitudinal anti-cracking analysis program, the result can be obtained as following:

$$P_{1cr} \subset (2175, 2388)\ \text{kN}, \quad P_{2cr} \subset (1255, 1452)\ \text{kN}$$

According to the prestress design: P_1 = 1562.4 kN × cos7.5° = 1549 kN, P_2 = 1562.4 kN

Therefore, the original design of the prestressed voided slab girder can not meet the requirement of longitudinal anti-cracking. Longitudinal cracks are expected to occur at the junction area between the web and bottom plates. According to the previous analysis results of the influential factors, the increase of bottom plate thickness can increase P_{2cr} effectively. Therefore, the original anchor end section design is modified, and the thickness of bottom plate is increased from 12 cm to 15 cm. After the modification, through the calculation, $P_{2cr} \subset$ (1695, 1895)kN, and it can meet the longitudinal anti-cracking requirement. This research result is finally adopted for the design improvement of this engineering project.

4.2 The girder of Jinhua national road bridge in Zhejiang Province

Fig. 12 shows the section of a prestressed voided slab girder with 20 m span used in Jinhua national road bridges of Zhejiang Province, China. Three bunches of five 1860 MPa-grade straight linear prestressed steel strands are located at the bottom plate. The total tensioning control force for tendons on the bottom plate is 2929.5 kN. The material constants are E = 3.45 × 10^4 MPa, G = 1.41 × 10^4 MPa and f_t = 1.71 MPa. After section equivalent, the geometry parameters for the analytical model are B = 1.195 m, δ_B = 0.20 m, T = 1.095 m, δ_T = 0.12 m, H = 0.9 m, δ_H = 0.135 m, and e = 0. There is not shear reinforcement settled on the shearing face, that is A_{s1} = 0. Being different from the example in part 4.1, prestress in this example is only applied on the bottom plate, leading to P_1 = 0. Then, it is obvious that the critical cracking state would occur according to the form of Model B. Therefore, the longitudinal anti-cracking analysis only needs to be made to Model B. According to the compiled longitudinal anti-cracking analysis program, the result can be obtained as following:

$$P_{1cr} \subset (1677, 2014)\ \text{kN} > P_1 = 0,\ P_{2cr} \subset (2236, 2583)\text{kN} < P_2 = 2929.5\ \text{kN}$$

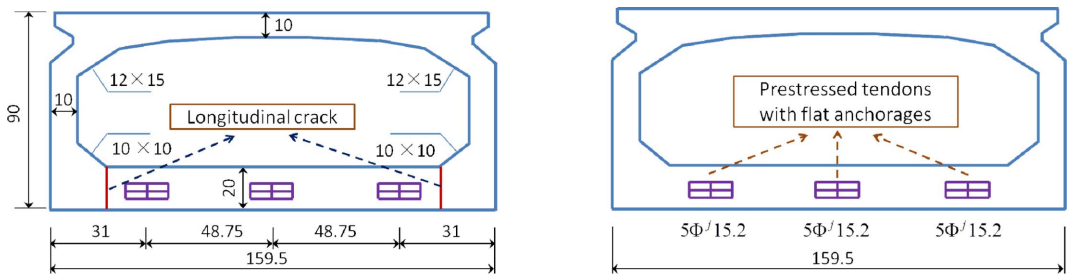

Fig. 12 Anchor end section of void slab girders in Jinhua National road bridges (unit: cm)

Therefore, the longitudinal anti-cracking requirement can not be met. The investigation about these bridges after construction also showed that most of them have longitudinal cracks at the bottom of the slab girder. This design was then suggested not to be adopted in the following construction of National road bridges in Zhejiang Province. Actually, if the thickness of the bottom plate is increased to 25 cm, the calculated result is $P_{2cr} \subset$ (3125, 3562)kN and it can meet the longitudinal anti-cracking requirement. Therefore, the longitudinal anti-cracking analysis is necessary for this kind of thin-walled void slab girders.

4.3 The girder of Ganzhou river-crossing bridge in Jiangxi Province

Fig. 13 shows the section of a prestressed voided slab girder with 30 m span used in Ganzhou river-crossing bridge of Jiangxi Province, China. In the precasting process of the voided slab girders, some longitudinal cracks occur in the near anchor end locations. Modified design should be made to improve the longitudinal anti-cracking ability of the girder.

As shown in Fig. 13, three bunches of four 1860 MPa-grade prestressed steel strands are located at the web plate, with bending angles of 12°, 8° and 2°, respectively. The tensioning control force for each bunch of tendons is 781.2kN. There is no prestressed tendon on top and bottom plates. Then, P_1 = 781.2 kN × (cos12°+ cos8°+ cos2°) = 2318 kN, and P_2 = 0. The material constants are $E = 3.45 \times 10^4$MPa, $G = 1.41 \times 10^4$ MPa, and f_t = 1.71 MPa. The equivalent geometry parameters for analytical model are B = 0.43 m, δ_B = 0.12 m, T = 0.43 m, δ_T = 0.12 m, H = 1.2 m, δ_H = 0.2 m, and e = 0. Four shearing reinforcements is settled along the shearing face, with the line spacing 10 cm and the diameter 12 mm, that is $A_{g1} = A_{g2}$ = 113 mm^2.

Since there is only prestress on the web plate, it can be determined that the critical cracking state would occur according to the form of Model A. Moreover, it should be noted that the geometry and prestress distribution is not only left-right symmetrical, but also nearly up-down symmetrical (without considering the negligible influence of tendon angle and web shape). Therefore, the stress sate of upper and lower shearing faces should be the same, and they would come to the critical state at the same time, which means ρ = 1. So the exact value of P_{1cr} can be calculated. According to Eq. (15) and Eq. (16), P_{1cr} = 1924 kN< P_1 = 2318 kN. Therefore, longitudinal cracks are sure to occur along the shearing surface. The most effective measure to improve P_{1cr} is to increase the

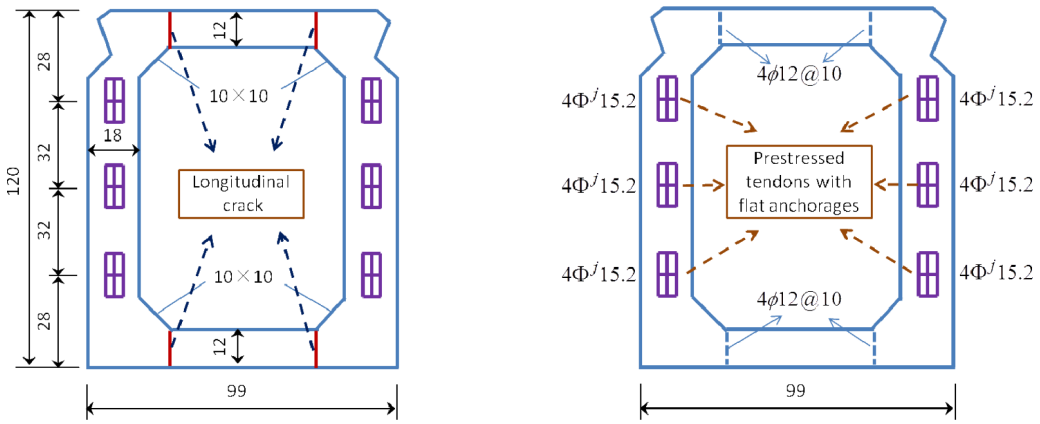

Fig. 13 Anchor end section of void slab girders in Jinhua National road bridges (unit: cm)

thickness of the web plate. When it is increased from original 18 cm to 25 cm, the calculated result is $P_{1cr} = 2638$ kN which can meet the longitudinal anti-cracking requirement. This modification is finally adopted in this design.

5. Conclusions

(1) The plate thickness of void slab girders is usually designed to be small with the adoption of flat anchorage system. Meanwhile, large prestress is applied to the anchor end section, leading to the great shear stress at the junction area between web and bottom (top) plates. As a result, the longitudinal anti-cracking problem in the anchor end area can not be neglected. This paper presented two possible models for this problem, and a practical longitudinal anti-cracking analysis method is constructed based on the differential element approach.

(2) The major factors that have influence on the longitudinal anti-cracking capability of prestressed voided slab girders are the dimension of the anchor end section (thickness of the bottom, web and top plate), and the eccentricity of the prestress imposed on the web plate. The increase of shear reinforcement on the shearing face has little influence on the improvement of the critical cracking prestress.

(3) Generally, when making the longitudinal anti-cracking analysis, both Model A and B are usually necessary to be analyzed. The final critical cracking prestress should be the minimum value between the solutions of the two models. However, when the prestress is only applied to web (bottom) plates, only Model A (B) need to be analyzed, since the other analytical model can be determined not to happen at this time.

(4) The presented method is verified in prestressed voided slab girders of three engineering examples: Suqian-Huaian Expressway in Jiangsu Province, Jinhua national road bridge in Zhejiang Province, and Ganzhou river-crossing bridge in Jiangxi Province. The longitudinal anti-cracking ability of these girders is calculated and checked. Results show that the original design can not meet the requirement. This also demonstrates that the longitudinal anti-cracking analysis is necessary for the anchor end design of voided slab girders. Design improvement is determined according to the research of this paper and adopted in these engineering projects.

Acknowledgements

This research is sponsored by Jiangsu Province Natural Science Foundation of China (BK2010428), Fresh Teacher Research Foundation of Chinese Education Ministry (20090092120017), and Research Foundation of Southeast University in China (KJ2009355). The support is gratefully acknowledged.

References

Connor, A.O. and Enevoldsen, I.B. (2008), "Probability based modeling and assessment of an existing post-tensioned concrete slab bridge", *Eng. Struct.,* **30**(5), 1408-1416.

Díaz, J., Hernández, S., Fontán, A. and Romera, L. (2010), "A computer code for finite element analysis and

design of post-tensioned voided slab bridge decks with orthotropic behaviour", *Adv. Eng. Soft*, **41**(7-8), 987-999.

Jaeger, L.G., Bakht, B. and Tadros, G. (1998), "Equivalent area of voided slabs", *Can. J. Civil. Eng.*, **25**(4), 797-801.

Jáuregui, D.V., Licon-Lozano, A. and Kulkarni, K. (2010), "Higher level evaluation of a reinforced concrete slab bridge", *J. Bridge Eng.,* **15**(2), 172-182.

John, H.M. and Kurtis, D.F. (2005), *Numerical Methods Using MATLAB*, Prentice Hall, Englewood Cliffs, NJ.

Lounis, Z. and Cohn, M.Z. (1995), "Computer-aided design of prestressed concrete cellular bridge decks", *Microcomput. Civil Eng.*, **10**(1), 1-11.

Mari, A.R. and Montaner, J. (2000), "Continuous precast concrete girder and slab bridge decks", *Proceedings of the ICE: Structures and Buildings*, **140**(3), 195-206.

O'Brien, E.J. and Keogh, D.L. (1998), "Upstand finite element analysis of slab bridges", *Comput. Struct.,* **69**(6), 671-683.

Qaqish, M., Akawwi, E., Fadda, E. and Qaqish, M. (2009), "Comparison between computed shearing forces by AASHTO specifications and finite element method of two continuous spans of voided slab bridge", *WSEAS Transactions on Information Science and Applications*, **6**(4), 621-636.

Scollard, C.R. and Bartlett, F.M. (2004), "Rehabilitation criteria for post-tensioned voided-slab bridges", *Can. J. Civil. Eng.*, **31**(6), 977-987.

Sen, R., Issa, M. and Gergess, A. (1993), "Collapse load analysis of continuous, posttensioned voided slab bridge models", *J. Struct. Eng., ASCE,* **119**(6), 1825-1843.

Zhao, Z., Jiang, X.D. and Huo, D. (2007), "Single slab load analysis of pre-stressed concrete hollow slab based on destructive test", *Journal of Beijing University of Technology*, **33**(5), 498-502. (in Chinese)